Control of multi-Level Voltage Source Converters Integrating a Wind Turbine System into the Grid

E. Hamatwi[1*]
Department of Electrical Engineering
University of KwaZulu-Natal
Durban, 4001, South Africa
esterhamatwi@gmail.com

I E Davidson[2]
Department of Electric Power Engineering
Durban University of Technology
Durban, 4001, South Africa
InnocentD@dut.ac.za

M N Gitau[3]
Department of Electrical Engineering
University of Pretoria
Pretoria, 0002, South Africa
njoroge.gitau@up.ac.za

***Abstract*—In recent years, wind energy has proven to be the most competitive and environmental friendliest renewable energy (RE) source for generating electricity. Wind farms are more likely to be located far from the load centres, and hence the generated power has to be transmitted over long distances. A high voltage direct current (HVDC) transmission system increases the transmission capacity, improves the system stability, and possesses lower transmission losses. Therefore, it is the preferred means for power delivery over long distances compared to the high voltage alternating current transmission system. In this paper, a 690V, 2MW wind turbine is modelled to be integrated into a 33kV AC grid via a 3-level Neutral-Point-Clamped Voltage Source Converter-based HVDC transmission system. Three control schemes were implemented: a pitch-angle controller, a controller applied to the generator-side converter, and a controller applied to the grid-side converter. The proposed wind energy conversion system and control schemes were implemented in MATLAB/SIMULINK and simulations were carried out to analyse the performance of the system.**

Keywords—Wind Energy, Voltage Source Converters, High Voltage Direct Current, Vector Control, PMSG

I. Introduction

Wind energy has recently been considered as a fast growing RE source mainly due to the growth in the size of commercially available wind turbine designs[1]. A number of studies have been carried out focusing on integrating wind turbines/farms into the grid via 2-level Voltage Source Converter (VSC) topologies. These VSC topologies have proven to be reliable, robust, and their configuration is simple and easy to implement. However, they have drawbacks such as high switching losses, and they synthesize voltages with poor waveform quality, thus they require a large number of filtering elements[2]. Conversely, multi-level VSCs are associated with lower switching losses, higher overall efficiency, and they synthesize voltages with better waveform quality thus cutting down on the size and on the number of filtering elements. Considering the intermittency of wind, wind energy conversion systems (WECS) needs to be interfaced with the grid via power electronic converters to synchronize the two systems [2], [3].

The direct and vector-oriented control (VOC) are the well-developed control techniques used to control the active and reactive power in WECS and they are discussed further in the literature[4].

Freire et. al [5] carried out a comparative study on the direct and vector control strategies. It was concluded that, although the direct control technique has a fast dynamic response and it is easy to implement, vector control technique has a better performance due to lower current distortions, and higher overall efficiency. The VOC is made up of a dual-loop control structure: a slow outer control loop and a fast inner current control loop. The outer control loops are made up of controllers that provide the reference values of the inner current controllers. The VOC technique is implemented in this study.

II. Detailed System Mathematical Modelling

A. Operating Principle of a Wind Turbine System

The amount of power extracted by a wind turbine from the wind resource is related to the wind speed by (1) [1], [2]

$$P_m = \frac{1}{2}\rho A C_p(\lambda,\beta) v_w^{\,3} \tag{1}$$

Where: ρ is the air density above sea level, A is the area swept by the rotor blades [m^2], v_w is the wind speed upstream of the rotor [m/s] and C_p is the aerodynamic power coefficient dependent on the blade-pitch-angle β [degrees] and tip speed ratio λ.

B. Drive-Train Model

A drive train is responsible for transmitting torque from the low-speed shaft to the high-speed shaft [2], [6], [7]. The swing equation representing a single-mass drive train is defined by (2) [6]

$$\frac{d\omega_r}{dt} = \frac{T_m - T_e - \omega_r B_{eq}}{J_{eq}} \tag{2}$$

Where: T_m is the aerodynamic torque, T_e is the electromagnetic torque [N.m], B_{eq} is the equivalent damping coefficient [N.m/s] and J_{eq} is the equivalent rotational inertia of the generator [kg.m^2].

C. Mathematical Modelling of a Permanent Magnet Synchronous Generator (PMSG)

The detailed mathematical modelling and equations describing a PMSG have been discussed in more details in Kundur[8].

978-1-5090-3388-1/16/$31.00 ©2016 IEEE

Equation (3) represents the PMSG's stator voltages in dq-synchronous reference frame [6]

$$V_{sd} = R_s i_{sd} + L_{sd}\frac{di_{sd}}{dt} - \omega_e L_{sq} i_{sq}$$
$$V_{sq} = R_s i_{sq} + L_{sq}\frac{di_{sq}}{dt} + \omega_e (L_{sd} i_{sd} + \psi_f) \quad (3)$$

Where; V_{sd} and V_{sq} are the d- and q-component of the stator voltage [V], respectively; i_{sd} and i_{sq} are the d- and q-component of the stator current [A], respectively; L_{sd} and L_{sq} are the d- and q-component of the stator's self-inductances [H], respectively; R_s is the stator winding resistance [Ω]; ψ_f is the permanent magnetic flux [Wb], and ω_e is the electrical rotating speed [rad/s] of the generator.

D. 3-Level NPC VSC Mathematical Modeling

Fig.1 shows a schematic diagram of one arm of a 3-level NPC multilevel converter topology.

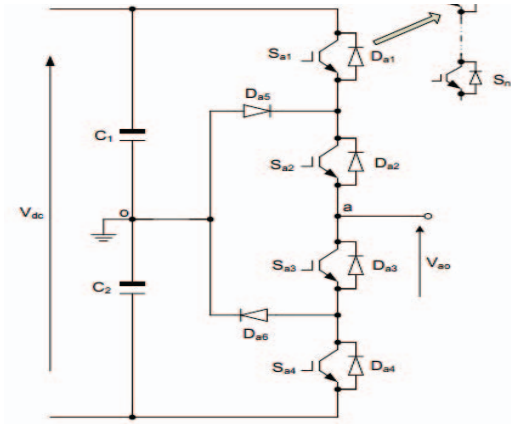

Fig. 1. 3-Level NPC VSC Topology[9]

A 3-level NPC converter has four switches per phase/leg and it generates three voltage levels, namely: $V_{dc}/2$, 0 and $-V_{dc}/2$.

The minimum DC voltage level required to avoid converter saturation when using PWM is given by (4) [9], [10]

$$V_{dc} = 2\sqrt{\frac{2}{3}} \times V_{LL} \quad (4)$$

Where V_{LL} is the line-to-line voltage.

Therefore, using the wind turbine's rated line-to-line voltage of 690V, the DC-link voltage is equal to 1126.77V.

The converter's output terminal voltage is related to the steady-state modulation index m and DC-link voltage V_{dc} by (5)[9]

$$V_m = \frac{1}{2}\sqrt{\frac{3}{2}} \times V_{DC} \times m \quad (5)$$

Saturation effects are avoided when the converter operates within the linear modulation index range. This is ensured by limiting the PWM modulation index to 1, that is $0<m\leq 1$[2], [9].

In this study, the modulation index is chosen to be 0.9 as this value is employed in most commercial applications[10]. Therefore, the converter output terminal voltage is equal to 620.62V.

III. System Controller's Modeling

A. Pitch-Angle Control

1) Controller Objective

The aim of the pitch-angle controller is to protect the wind turbine (WT) from over-speeding during high wind speeds[11]. This is ensured by increasing the pitch-angle to turn the wind turbine blades away from the striking wind. As a result, the aerodynamic power coefficient C_p is reduced thereby shedding off the aerodynamic power extracted from the wind source at that instant.

2) Derivation of the Transfer Functions

Fig. 2 (a), (b), and (c) presents the block diagram of the pitch-angle controller, the pitch-actuator model, and the complete block diagram of the pitch-angle controller, respectively.

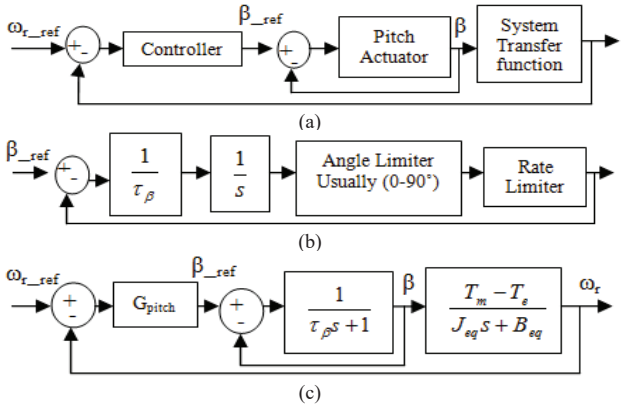

Fig. 2. (a) Pitch Angle Control Loop; (b) Pitch Actuator block diagram; (c) Complete block diagram of the pitch angle controller

The pitch-actuator system's closed-loop transfer function is given by (6)

$$G_{actuator,cl}(s) = \frac{1}{\tau_\beta s + 1} \quad (6)$$

Where τ_β is the time constant of the actuator system [2], [12].

The system transfer function block in Fig. 2(a) represents the aerodynamic and mechanical system of the wind turbine system. Its transfer function is derived using the swing equation given by (2).

Taking the Laplace transform of (2) gives (7) representing the system transfer function.

$$\omega_r (J_{eq} s + B_{eq}) = T_m - T_e = \frac{T_m - T_e}{J_{eq} s + B_{eq}} \quad (7)$$

From Fig. 2(c), the pitch-angle controller's closed-loop transfer function is represented by (8)

$$G_{pitch\_cl}(s)=\frac{G_{pitch}(s)(T_m-T_e)}{(\tau_\beta s+1)(J_{eq}s+B_{eq})+G_{pitch}(T_m-T_e)} \quad (8)$$

B. Modelling of the Generator-side Converter Controller

1) Controller Objective

The controller applied to the generator-side converter is responsible for stabilizing the DC-link voltage and for keeping the stator voltage constant at its rated value which ensures that there is no risk of over-voltages.

2) Derivation of the Transfer Functions

a) Inner Current Control Loop

Fig.3 (a) and (b) shows the initial and final inner current control loops for the generator-side converter controller, respectively.

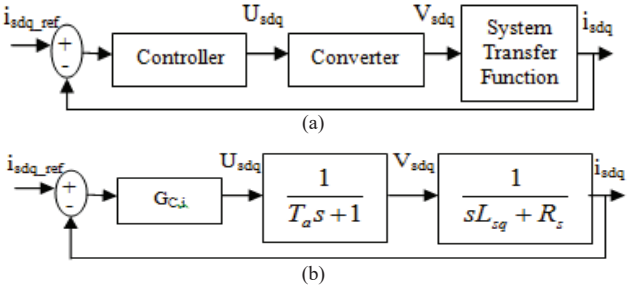

Fig. 3. Inner current control loop for the generator-side converter, (a) Initial control block; (b) Complete block diagram

A converter is usually considered as an ideal transformer with a time delay caused by the switching of the converter switches. The delay time is equal to the half of the switching time. The transfer function of the converter block is therefore given by (9) [13];

$$Y(s)=\frac{1}{T_a s+1} \quad (9)$$

Where $T_a=\frac{T_{switch}}{2}=\frac{1}{2f_{switch}}$, is the time delay in seconds.

The system's behavior is governed by the equations that represent the PMSG's stator voltages in dq-synchronous reference frame given by (3). The d- and q-components of the stator voltage have a speed or frequency induced term $\omega_{se}L_{sq}i_{sq}$ and a speed or frequency and a flux induced term $\omega_{se}(L_{sd}i_{sd}+\psi_f)$, respectively, which ensures cross-coupling between the two axes. To obtain a good control performance, it is required to decouple the d- and q- axis [10]. Removing the cross-coupling terms gives (10) which represents the system's transfer function in Fig. 3(a).

$$V_{sd}=R_s i_{sd}+L_{sd}\frac{di_{sd}}{dt}$$
$$V_{sq}=R_s i_{sq}+L_{sq}\frac{di_{sq}}{dt} \quad (10)$$

Taking the Laplace transformation of (10) gives (11) relating the output stator current to the stator voltage.

$$\frac{i_{sd}(s)}{V_{sd}(s)}=\frac{i_{sq}(s)}{V_{sq}(s)}=\frac{1}{sL_{sdq}+R_s} \quad (11)$$

From Fig. 3(b), the closed-loop transfer function of the inner current control loop is represented by (12)

$$G_{i,cl}(s)=\frac{G_{C,i}(s)}{(sTa+1)(sL_{sdq}+R_s)+G_{C,i}(s)} \quad (12)$$

b) Outer Controller Loops

- **DC-Link Voltage Control Loop**

Fig. 4 (a) and (b) shows the initial and final block diagram of the DC-link voltage control loop, respectively. The outer controller block generates the d-component of the reference stator current that is fed into the inner current control loop.

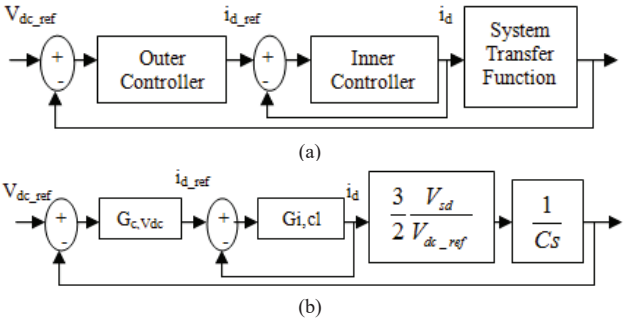

Fig. 4. DC-link voltage controller loop, (a) Initial control block; (b) Final control block

Considering the DC-link capacitor node, the DC-side dynamics are described by (13) [14].

$$I_C=C\frac{dV_{dc}}{dt}$$
$$I_C=I_{dc}-I_L \quad (13)$$

Where, I_C, I_{dc} and I_L, are the capacitor, DC-link and load current, respectively.

The power on the DC side is given by (14)

$$P_{dc}=V_{dc}I_{dc} \quad (14)$$

Using the d-q axis theory, the instantaneous real and reactive power of the PMSG are described by (15) [10].

$$P_{gen}=\frac{3}{2}(V_{sd}i_{sd}+V_{sq}i_{sq})$$
$$Q_{gen}=\frac{3}{2}(V_{sq}i_{sd}-V_{sd}i_{sq}) \quad (15)$$

Considering that the DC-link voltage controller ensures that the power on the AC-side is equal to the power on the DC-side. The system transfer function is derived as follow:

$$P_{gen}=P_{dc}$$
$$\frac{3}{2}V_{sd}i_{sd}=V_{dc}I_{dc}$$

Therefore (13) becomes (16)

$$C\frac{dV_{dc}}{dt} = \frac{3}{2}\frac{V_{sd}}{V_{dc}} i_{sd} - I_L \quad (16)$$

The only input of interest into the system transfer function block is i_{sd} and I_L acts as a disturbance. Therefore, the simplified equation representing the system's transfer function is given by (17)

$$C\frac{dV_{dc}}{dt} = \frac{3}{2}\frac{V_{sd}}{V_{dc\_ref}} i_{sd} \quad (17)$$

Taking the Laplace transform of (17) gives (18) that relates the d-component of the stator current to the DC-link voltage.

$$\frac{V_{dc}}{i_{sd}(s)} = \frac{3}{2}\frac{V_{sd}}{V_{dc\_ref}} \times \frac{1}{Cs} \quad (18)$$

From Fig. 4(b), the DC-link voltage controller's closed-loop transfer function is represented by (19)

$$G_{v,cl}(s) = \frac{3V_{sd}G_{C,Vdc}(s)G_{i,cl}(s)}{2V_{dc\_ref}Cs[(sTa+1)(sL_{sd}+R_s)+G_{C,c}(s)]+3V_{sd}G_{C,Vdc}(s)G_{i,cl}(s)} \quad (19)$$

- **Stator Voltage Control Loop**

Fig. 5(a) and (b) shows the initial and final block diagrams of the stator voltage control loop. The outer controller block generates the q-component of the reference stator current that is fed into the inner current control loop.

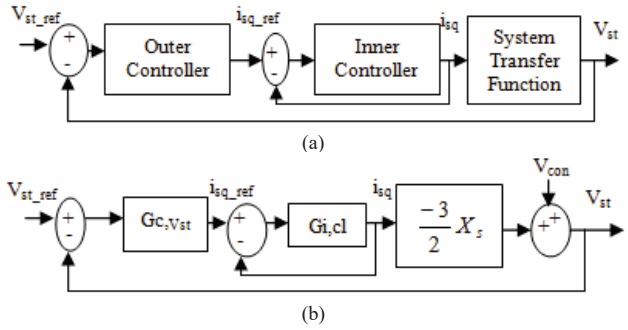

Fig. 5. Stator voltage control loop, (a) Initial control block; (b) Final control block

The system transfer function is governed by the voltage drop across the stator reactance which is described by (20) [10]

$$\Delta V = V_s - V_{con} = \frac{R_s P_{gen} + X_s Q_{gen}}{V_s} \quad (20)$$

Where, V_s is the stator voltage, V_{con} is the converter voltage, R_s is the stator winding resistance and X_s is the synchronous reactance which is equal to ω_e $(L_{sd}+L_{sq})$. Assuming that $X_s >> R_s$ for the stator reactance, the voltage drop depends only on the reactive power flow. Therefore, from Fig. 5(b), the stator voltage controller's closed-loop transfer function is given by (21)

$$G_{v_{st},cl}(s) = \frac{(-3X_s + V_{con}) \times G_{C,v_{st}}(s)G_{i,cl}(s)}{2[(sTa+1)(sL_{sq}+R_s)+G_{i,cl}(s)]-(3X_s+V_{con})\times G_{C,v_{st}}(s)G_{i,cl}(s)} \quad (21)$$

C. Modelling of the Grid-side Converter Controller

1) Controller Objective

The objective of the controller applied to the grid-side converter is to ensure that optimal power is extracted from the wind resource during low wind speeds. This is ensured by controlling the generator's rotor speed. The controller is also used to control the reactive power fed into the grid to ensure unity power factor.

2) Derivation of the controllers' Transfer Functions

a) Inner Current Control Loop

The derivation of the transfer function of the grid-side converter's inner current control loop follows the same procedure used to derive the transfer function of the generator-side converter's inner current control loop.

Furthermore, their transfer functions are similar with only a few modifications. Therefore, the inner current controller's closed-loop transfer function is given by (22)

$$G_{C,cl}(s) = \frac{G_{C,i}(s)}{(sTa+1)(sL_t+R_t)+G_{C,i}(s)} \quad (22)$$

b) Outer Control Loops

- **Active Power Control Loop/MPPT Control Loop**

Over the past years, various maximum power point tracking (MPPT) techniques have been developed and they are discussed in the literature[4]. In this study, the Optimal Relationship-Based (ORB) control is employed to achieve MPPT because of its fast response, enhanced power smoothing capability and simplicity[1]. The power is controlled indirectly by continuously changing the rotor speed ω_r with respect to the change in the wind speed v_w. The equation relating the optimal power to the optimal rotor speed is given by (23)[1], [15]:

$$P_{opt} = \frac{1}{2}\rho A C_{P_{opt}} \left(\frac{\omega_{r_{opt}} \times r}{\lambda_{opt}}\right)^3 \quad (23)$$

The output power P_{opt} from the MPPT stage serves as an input into the outer active power control loop. The outer controller block generates the d-component of the reference current that is fed into the inner current control loop. Fig. 6(a) and (b) shows the initial and final active power control loops.

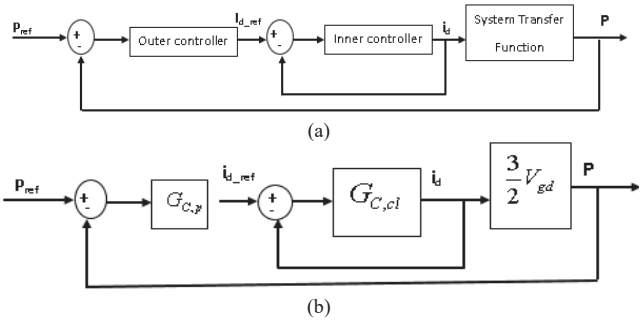

Fig. 6. Active power control loop, (a) Initial control loop; (b) Final control loop

Using the d-q axis theory, and VOC technique, the instantaneous real and reactive power transferred from the converter into the grid are described by (24)

$$P = \frac{3}{2} V_{gd} i_d \qquad (24)$$
$$Q = -\frac{3}{2} V_{gd} i_q$$

Therefore, the system transfer function in Fig. 6(a) is given by (25)

$$\frac{P}{i_d} = \frac{3}{2} V_{gd} \qquad (25)$$

From Fig. 6(b), the active power controller's closed-loop transfer function is represented by (26)

$$G_{P,cl}(s) = \frac{3V_{gd} G_{C,p}(s) G_{C,cl}(s)}{3V_{gd} G_{C,p}(s) G_{C,cl}(s) + 2} \qquad (26)$$

- **Reactive Power Control Loop**

Fig.7 (a) and (b) shows the initial and final reactive power control loops, respectively. The outer controller block generates the q-component of the reference current that is fed into the inner current control loop.

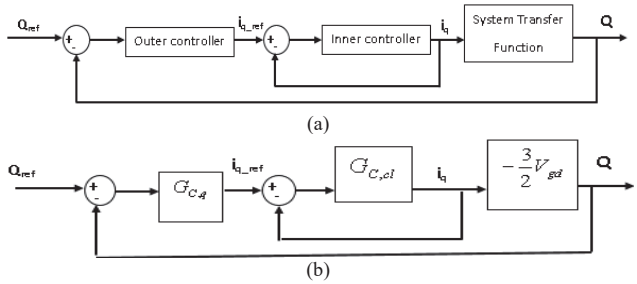

Fig. 7. Reactive Power Control Loop, (a) Initial control loop, (b) Final control loop

The system transfer function is derived from (24). Therefore, it is given by (27)

$$\frac{Q}{i_q} = -\frac{3}{2} V_{gd} \qquad (27)$$

From Fig. 7(b), the reactive power controller's closed-loop transfer function is represented by (28)

$$G_{Q,cl}(s) = -\frac{3V_{gd} G_{C,q} G_{C,cl}}{3V_{gd} G_{C,q} G_{C,cl} + 2} \qquad (28)$$

IV. Results and Discussions

The wind speed was made to vary to analyse its impact on the performance of the system. Fig. 8 shows the variation in wind speed from the WT's cut-in wind speed (4m/s) to the WT's rated wind speed (13m/s) at 0.8s and it keeps increasing thereby exceeding the rated wind speed.

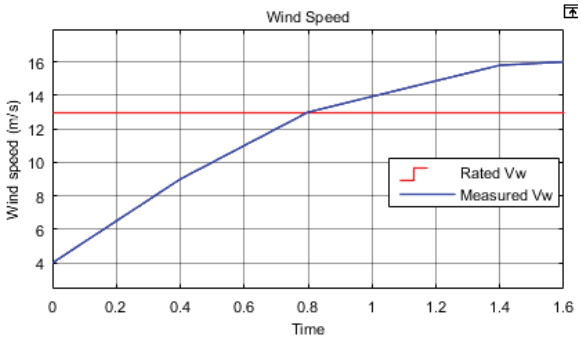

Fig. 8. Wind Speed

Fig. 9 (a) and (b) shows the changes in the pitch-angle and the power coefficient *Cp* relative to the change in wind speed, respectively.

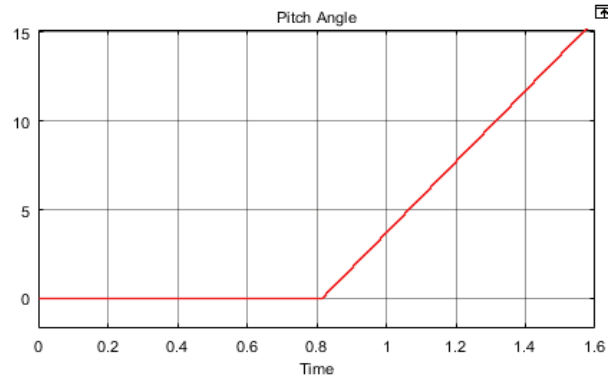

(a)

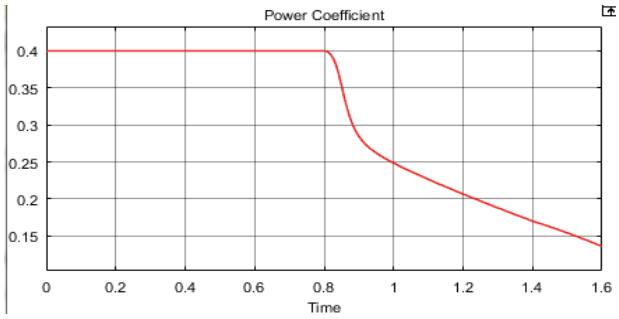

(b)

Fig. 9. (a) Pitch angle; (b) Power Coefficient

From Fig. 9 (a), it is observed that the pitch-angle controller remains inactive when the wind speed is lower than the WT's rated wind speed (13m/s) and only gets activated when the wind speed exceeds 13m/s. Fig. 9 (b) shows that the power coefficient C_p increases and remains constant at the rated value. However, as the wind speed exceeds 13m/s, the power coefficient C_p starts decreasing. This is possible because of the pitch-angle control technique.

Fig. 10 shows the generated aerodynamic power

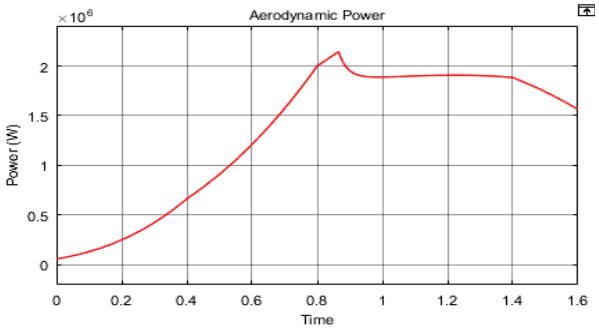

Fig. 10. Aerodynamic Power

It is observed that when the wind speed is below the WT's rated wind speed (13m/s), the power generated from the WT tracks the optimal power curve to ensure MPPT. At 13m/s, the aerodynamic power is approximately equal to 2MW which is the WT's rated power. However, as the wind speed exceeds 13m/s, the power overshoots and then begins dropping and remains within the rated value. This is made possible by the pitch-angle control technique.

Fig.11 (a) and (b) illustrates the stator voltage and stator current waveforms, and the grid voltage and grid current waveforms, respectively.

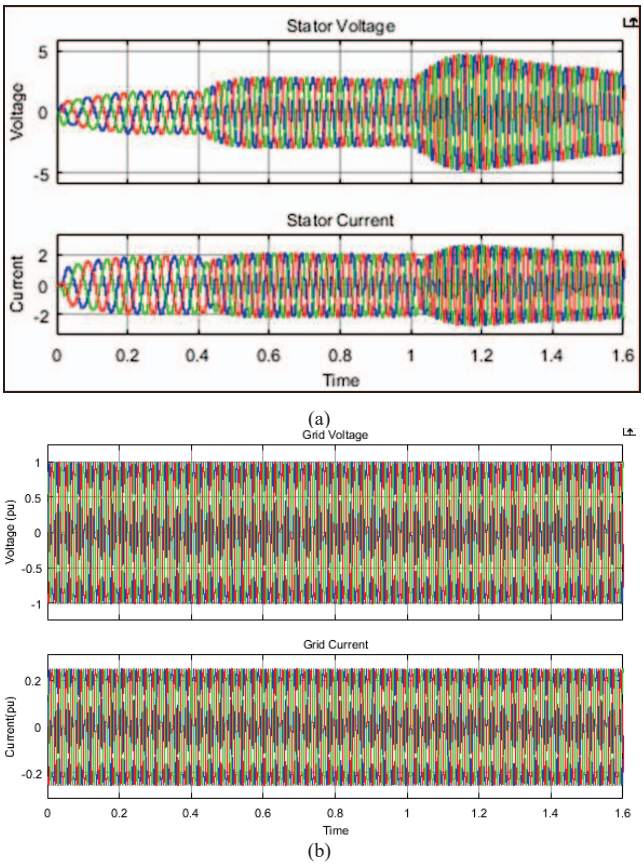

Fig. 11. (a) The stator's three-phase voltage and current waveforms; (b) Grid's three-phase voltage and current waveforms

Fig. 11(a) indicates that the stator voltage and current increase as the wind speed increases. Conversely, the grid voltage and current remains constant.

Fig.12 represents the DC-link voltage waveform. It is observed that the DC link voltage remains fixed at 1126V as expected.

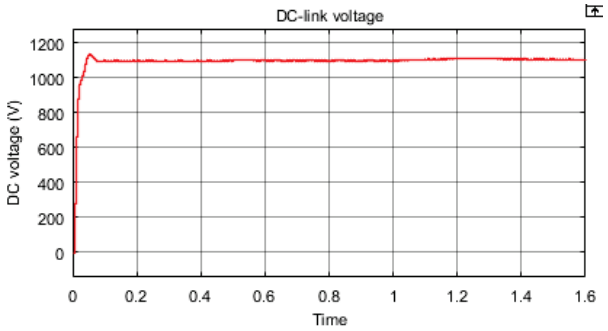

Fig. 12. DC-Link Voltage

V. Conclusion

The proposed wind energy conversion system and control schemes were successfully implemented in MATLAB/SIMULINK. Based on the simulations, the controller applied to the grid-side converter ensured MPPT when the wind speed was lower than the WT's rated wind speed (13m/s). Moreover, it was observed that the power coefficient C_p remained constant at its rated value and only started dropping when the wind speed exceeded 13m/s. This was possible because of the pitch-angle control technique, and hence, the amount of power extracted from the wind resource by the wind turbine decreased to protect the WT from sudden wind gusts.

References

[1] S. M. Tripathi, A. N. Tiwari, and S. Deependra, "Grid-integrated permanent magnet synchronous generator based wind energy conversion systems: A technology review," *Renewable and Sustainable Energy Reviews,* vol. 51, pp. 1288-1305, 2015.

[2] E. Hamatwi, I. E. Davidson, M. N. Gitau, and G. P. Adam, "Modeling and Control of Voltage Source Converters for Grid Integration of a Wind Turbine System," in *2016 IEEE PES Power Africa Conference*, Livingstone, Zambia, 2016.

[3] Z. Chen and J. M. Guerrero, "A review of the state of the art of power electronics for wind turbines," *IEEE Transaction on Power Electronics,* vol. 24, pp. 1859-1875, August 2009.

[4] S. Li, T. A. Haskew, and L. Xu, "Conventional and novel control designs for direct driven PMSG wind turbines," *Electric Power Systems Research,* vol. 80, pp. 328-338, 2010.

[5] N. Freire, J. Estima, and A. Cardoso, "A Comparative Analysis of PMSG Drives Based on Vector Control and Direct Control Techniques for Wind Turbine Applications," *Electrical Review,* vol. 88, pp. 184-187, 2012.

[6] G. Vazquez, D. Aguilar, and G. Azevedo, "Modeling of a variable speed wind turbine with a permanent magnet synchronous generator," in *IEEE International Symposium on Industrial Electronics (ISIE 2009)*, Seoul Olympic Parktel, Seoul, Korea, pp. 734-739, 2009.

[7] J. F. Hall and D. Chen, "Dynamic Optimization of Drivetrain Gear Ratio to Maximize Wind Turbine Power Generation—Part 1: System Model and Control Framework," *Journal of dynamic systems, measurement, and control,* vol. 135, pp. 011-016, 2013.

[8] P. Kundur, *Power System Stability and Control*, 1 ed. New York: McGraw-Hill Education, 1994.

[9] G. P. Adam, *Voltage Source Converter: modulation, modelling, control and applications in power systems*, 1 ed. Charleston, SC, USA: CreateSpace Independent Publishing Platform, 2014.

[10] T. W. Shire, "VSC-HVDC based Network Reinforcement," Masters, Department of High-Voltage Components and Power Systems, Delft University of Technology, 2009.

[11] I. Hamzaoui, F. Bouchafaa, and A. Talha, "Pitch Angle Control for Variable Speed Wind Turbines with Doubly Fed Induction Generators," *Journal of Electrical Engineering,* pp. 1-8, 2011.

[12] N. A. Orlando, M. Liserre, and R. Mastromauro, "A survey of control issues in PMSG-based small wind-turbine systems," *Industrial Informatics,* vol. 9, pp. 1211-1221, 2013.

[13] O. Gomis-Bellmunt, A. Junyent-Ferre, A. Sumper, and J. Begas-Jane, "Control of a Wind Farm Based on Synchronous Generators With a. Central HVDC-VSC Converter," *IEEE Transactions on Power Systems,* vol. 26, pp. 1632-1640, 2011.

[14] G. P. Adam, "Quasi Two-Level Operation of a Five-Level Diode Clamped Inverter," PhD Thesis, Electrical and Electronic Engineering Department, University of Strathclyde, Glasgow, UK, 2007.

[15] A. D. Hansen and G. Michalke, "Modelling and Control of variable speed Multi-pole Permanent Magnet Synchronous generator Wind Turbine," *Wind Energy,* vol. 11, pp. 537-554, 2008.

APPENDICES

TABLE I. WIND TURBINE PARAMETERS

Parameters	Values
Rated Power (MW)	2
Cut-In wind speed (m/s)	4
Rated wind speed (m/s)	13
Cut-out wind speed (m/s)	25
Number of rotor blades	3
Rotor area (m2)	4587
Rotor diameter (m)	76.42
Rated speed (rpm)	19
Air density (kg/m2)	1.225
Maximum Cp	0.4
Maximum λ	6.92

TABLE II. PERMANENT MAGNET SG PARAMETERS

Parameters	Value
Generator type	PMSG
Rated real power, P (MW)	2
Rated apparent power, S (MVA)	2.24
Rated L-L voltage, V_{L-L} (V), rms	690
Rated phase voltage, V_{ph} (V), rms	398.37
Rated power factor, pf	0.89
Rated rotor speed, ω_{rated}(rpm)	22.5
Pole pairs, n_p	26
Permanent magnet flux linkage, ψ_f (Wb)	4.971
Stator winding resistance, R_s (mΩ)	0.821
Stator d-axis inductance, L_{ds} (mH)	1.573
Stator q-axis inductance, L_{qs} (mH)	1.573